Application of spin echo technique to Bose-Einstein condensates: time evolution of the spins by simulating and computing the Gross-Pitaevskii equation

by

Araceli Venegas Gómez

Máster de Física Médica

Facultad de Ciencias
UNIVERSIDAD NACIONAL DE EDUCACIÓN A DISTANCIA

Supervisores: Dra. Cristina Santa Marta Pastrana
Prof. José Carlos Antoranz Callejo

December 2016

Copyright

Abstract

The principles of Nuclear Magnetic Resonance (NMR) can be understood thanks to the magnetic properties of the nuclei derived from the intrinsic spin and the orbital angular momentum, enabling a precise control on the dynamics of the nuclear spin system by means of radio-frequency (RF) pulses.

NMR has revolutionised the field of medical imaging, being one of the few techniques where no ionizing radiation is employed, besides ultrasound.

However, not exclusively medicine benefits from the outstanding applications of this physical phenomenon. Structural and chemical information of diverse atomic species can be likewise investigated through NMR.

Furthermore, in the recent cutting-edge research in quantum computing, magnetic resonance is an alternative technique to create the first quantum computer.

Moreover, the application of NMR to unique states of matter at very low temperatures explores the behaviour of the spins in different elements, revealing very interesting physical properties.

In this thesis, the application of an important and precise pulse sequence, spin echo, to a specific type of Bose-Einstein condensate, a spin-1 spinor, is studied. The interest of this work focusses on analysing the spin evolution when only the short range interaction constants are taking into account.

The simulations are computed applying numerical algorithms, by making use of GPELab, a $MATLAB^{®}$ toolbox developed to model non linear Schrödinger equations, the so called Gross-Pitaevskii equations. The techniques are explored more in detail, analysing the type of algorithm to be applied to compute the dynamics of the system.

These results can be implemented in numerous experimental possibilities, and open up a new alternative to apply NMR in systems at very cold temperatures.

Resumen

Los fundamentos de la Resonancia Magnética Nuclear (RMN, o NMR por sus siglas en inglés) se basan en las propiedades magnéticas de los núcleos atómicos, como el espín y el momento angular orbital, permitiendo un control preciso en la dinámica del sistema nuclear mediante pulsos de radio frecuencia (RF).

La RMN ha revolucionado el campo de la imagen médica, siendo una de las pocas técnicas que no implica radiaciones ionizantes, junto a la ecografía.

Sin embargo, no sólamente el campo de la medicina se beneficia de las increibles aplicaciones de este fenómeno físico. También la información estructural y química de diversas especies atómicas pueden investigarse utilizando RMN.

Además, en el innovador y puntero campo de la investigación en computación cuántica, la resonancia magnética se presenta como una de las posibles alternativas para crear el primer ordenador cuántico.

Por otra parte, la aplicación de la resonancia magnética en estados de la materia únicos que aparecen a temperaturas enormemente bajas, explora el comportamiento de los espines en diferentes elementos, revelando propiedades físicas de importancia inigualable.

En esta tesis se estudia la aplicación de una precisa secuencia de pulsos, llamada eco de espín, a un específico condensado de Bose-Einstein, un espinor de espín-1. El interés de este trabajo se centra en el análisis de la evolución de los espines con el tiempo, considerando sólo las interacciones de corto alcance.

Las simulaciones se han generado aplicando algoritmos numéricos, utilizando una herramienta en $MATLAB^{®}$ llamada GPELab, desarrollada para representar ecuaciones de Schrödinger no lineales, denominadas ecuaciones de Gross-Pitaevskii. Las técnicas empleadas se han descrito en detalle, analizando el tipo de algoritmo escogido para estudiar la dinámica del sistema.

Estos estudios pueden implementarse en numerosas posibilidades experimentales, ofreciendo una nueva alternativa al uso de RMN en el estudios de sistemas a muy bajas temperaturas.

Agradecimientos

En primer lugar quisiera agradecer a la Dra. Cristina Santa Marta Pastrana. Sin su apoyo y estímulo durante la supervisión, este proyecto no habría podido salir adelante.

Y al Prof. José Carlos Antoranz Callejo, por darme la oprtunidad de meterme en un campo desconocido al proponer este tema para la tesis.

Quiero dar las gracias de corazón a Romain Duboscq, unos de los creadores de la herramienta que he utilizado durante las simulaciones. Por las fructíferas discusiones por email, donde ha respondido todas y cada una de mis dudas, y ha sido generosamente servicial, ayudándome cuando ya pensaba que no había manera de sacar resultados.

Al resto de profesores y trabajadores de la UNED, que durante estos años han intentado facilitar las cosas para los que intentamos estudiar estando en el extranjero, gracias.

Quiero agradecer a toda esa gente, mis amigos y compañeros, que durante el tiempo que estuve en Alemania tuvieron la paciencia de entender que a veces tenía que darlo todo por los estudios, y que era difícil compaginarlo con el trabajo. Por su infinita paciencia, gracias.

No puedo terminar sin agradecer a mi familia, en cuyo apoyo constante he confiado a lo largo de toda mi vida.

Finalmente, quiero dar las gracias a Francois, por estar siempre ahí en los momentos de estrés y darme siempre su apoyo.

Gracias / Thank you / Merci / Danke

Araceli, Octubre 2016

Contents

List of Figures

List of Tables

Part I

Hypothesis and objectives

Chapter 1

Overview

1.1 Short background

The importance of Nuclear Magnetic Resonance (NMR) has been intensively demonstrated in several fields.

Magnetic Resonance Imaging (MRI), using the signal of the nuclei of hydrogen atoms for image generation [1–3], plays a key role to deliver a better diagnosis in numerous diseases or medical conditions. Nevertheless, there are other potential applications. Research in recent years in the field of condensed matter physics has focused on magnetic materials (e.g. high temperature superconductors), and the study of the interaction with magnetic fields is attracting widespread interest to numerous fields in the scientific community. Furthermore, the appliance of NMR in low temperature physics can reveal important new features. Initial attempts of using NMR on Bose-Einstein condensates (BEC) provide particular information that explores the inner behaviour of molecules and atoms [4–6].

An alternative approach to a general NMR technique is the simulation of a specific pulse sequence, which is well understood in the case of hydrogen for the generation of a MRI. There remains a need for an efficient method that can work in a more complex environment.

1.2 Objective of the thesis

The purpose of this study is to describe and discuss the spin time evolution simulating the Gross-Pitaevskii equation using the GPELab program [7] when applying the spin-echo technique to a specific Bose-Einstein condensate trapped in harmonic potential, focusing on the results by Yasunaga and Tsubota [5, 6].

1.3 Outline of the thesis

The structure of this thesis is organised as follows. Chapter 2 contains theoretical background material, with a general introduction to the atomic properties, Nuclear Magnetic Resonance, and pulse sequences, specially spin echo, before describing a Bose-Einstein condensate.

In Chapter 3 the methodology is presented with the Gross-Pitaevskii equation. At the end of the chapter the equation which will be used during the simulations is introduced.

In the next two chapters the investigation results are described in detail. Chapter 4 presents the numerical methods and tools, and the corresponding equation to be employed in the computation. In Chapter 5 the results are presented, targeting the spin evolution when a magnetic field varying in time is applied.

Finally, Chapter 6 concludes this project providing a discussion of the results and achievements of the thesis, with some directions for futures perspectives.

Part II

Introduction

Chapter 2

Theoretical Background

In this chapter I will outline the theoretical background of my research. In Section 1 the properties of the atom are reviewed, in Section 2 and Section 3 the concept of Nuclear Magnetic Resonance and pulse sequences, specially spin echo, are respectively discussed. In Section 4, the Bose-Einstein condensation is described.

2.1 The properties of the atom

The Earth has two motions and associated with each of them are two types of angular momentum – the orbital angular momentum of the motion around the Sun and the intrinsic angular momentum around its axis. The electron has similarly orbital angular momentum L (motion around the nucleus) and intrinsic angular momentum S, as if the electron was spinning around its axis [8]. The total angular momentum of the electron is then $J = L + S$.

The nucleus is treated as if it had only intrinsic angular momentum I, and it is not common to speak about the orbital momenta of the nucleons, but only about their spin. The contribution of all the nucleons spins to the total angular momentum of the nucleus is known as nuclear spin [2, 9].

The total angular momentum or atomic spin is then given by $F = I + J$.

In Table 2.1 there is a clear evaluation of the nuclear spins related to the mass and atomic numbers.

TABLE 2.1: Value of I. Source: Own elaboration based on [2, 10]

Mass number A	Atomic number Z	Value of I
Even	Even	0
Even	Odd	Integral value (1, 2, 3...)
Odd	Odd	Half-integral value (1/2, 3/2, 5/2,..)
Odd	Even	Half-integral value (1/2, 3/2, 5/2,..)

The response of a specific atomic species to an applied magnetic field is the foundation of magnetic resonance.

2.2 Basis of Nuclear Magnetic Resonance

All Nuclear Magnetic Resonance (NMR) sensitive nuclei carry magnetic dipole fields, which means that they behave like bar magnets (see Fig. 2.1). The origin of this magnetic behaviour is nuclear angular momentum and spin, as described in previous section.

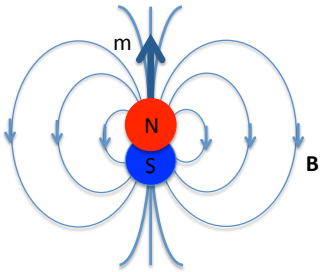

FIGURE 2.1: Example of a magnetic dipole.

In the absence of any external magnetic field, each particle will be oriented in an arbitrary direction (see Fig. 2.2). In the presence of a magnetic field, all the nuclear spins will align in a parallel or anti-parallel manner with the field direction. Spin-up spins have lower energy than spin-down (against the field) spins. Since lower energy states tend to be preferred, measurements on a set of spins in thermal equilibrium will show more nuclei in the spin-up than in the spin-down situation. The energy difference between the parallel

and antiparallel alignment is caused by the Zeeman interaction, and it is proportional to the external magnetic field strength, increasing with it [1–3, 11]:

$$\frac{N_1}{N_2} = e^{\frac{\Delta E}{k_B T}}, \tag{2.1}$$

with N_1 and N_2 the spins oriented parallel and antiparallel to the magnetic field B_0, k_B the Boltzmann constant and T the temperature of the system.

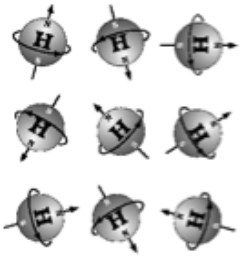

FIGURE 2.2: Protons oriented randomly acting like small magnets. [Source: http://www.simplyphysics.com]

When placed in a static and homogeneous magnetic field B_0, the nuclear spins will precess around the magnetic field direction. The frequency of precession, called the Larmor frequency (ω_0), is characteristic of the nuclei involved, and proportional to the strength of the external magnetic field:

$$\omega_0 = \gamma B_0, \tag{2.2}$$

with B_0 the magnetic field strength and γ the gyromagnetic ratio, a constant specific to the particular nucleus:

$$\gamma_n = g_n \frac{e}{2m_p}, \tag{2.3}$$

where m_p is the proton mass and g_n the g-factor of the nucleon (is a dimensionless quantity which characterizes the magnetic moment and gyromagnetic ratio related to the observed magnetic moment μ of a particle or nucleus).

The magnetic dipole moment, μ, of a single unpaired electron or nucleon is given by:

$$\mu = \gamma S, \tag{2.4}$$

being S the spin observable.

Table 2.2 lists the relevant constants for some elements commonly found in biological systems.

Element	Nuclear Composition		Nuclear Spin, I	Gyromagnetic Ratio β (MHz T^{-1})	% Natural Abundance	ω at 1.5 T (MHz)
	Protons	Neutrons				
^{1}H, Protium	1	0	1/2	42.5774	99.985	63.8646
^{2}H, Deuterium	1	1	1	6.53896	0.015	9.8036
^{3}He	2	1	1/2	32.436	0.000138	48.6540
^{6}Li	3	3	1	6.26613	7.5	9.39919
^{7}Li	3	4	3/2	16.5483	92.5	24.8224
^{12}C	6	6	0	0	98.90	0
^{13}C	6	7	1/2	10.7084	1.10	16.0621
^{14}N	7	7	1	3.07770	99.634	4.6164
^{15}N	7	8	1/2	4.3173	0.366	6.4759
^{16}O	8	8	0	0	99.762	0
^{17}O	8	9	5/2	5.7743	0.038	8.6614
^{19}F	9	10	1/2	40.0776	100	60.1164
^{23}Na	11	12	3/2	11.2686	100	16.9029
^{31}P	15	16	1/2	17.2514	100	25.8771
^{129}Xe	54	75	1/2	11.8604	26.4	17.7906

TABLE 2.2: Constants for selected nuclei of biological interest. Source: [2]

The net magnetic effect or magnetisation (M_0) of all the nuclear dipoles involved can be estimated by:

$$M_0 = \frac{N\gamma^2\hbar^2 B_0}{4k_B T}, \tag{2.5}$$

where $\hbar$ is the reduced Planck's constant and N the number of spins. It is important to deduce from Eq. 2.5 that the magnetic resonance signal will be stronger for substances with larger spin densities and when performed at higher magnetic fields.

When considering only a spin $S = 1/2$ in a magnetic field aligned with the z-axis, the following Hamiltonian (the energy of the system) is obtained in accordance with [1]

$$\hat{H} = -\mu B = -\left(-g_x \frac{e}{2m_x} S\right) B = \omega S, \tag{2.6}$$

where g_x denotes the g-factor for either the electron or the nucleon. Therefore, the energy is proportional to the z-component of the spin:

$$\hat{H} = \omega S_z. \tag{2.7}$$

As mentioned before, the net magnetic dipole moment will be pointing along B_0, as more spin-up nuclei in thermal equilibrium are found, consequently the equilibrium magnetisation is entirely along the z-axis [1–3, 11].

2.2.1 Free induction decay

A deviation from the equilibrium orientation to influence the magnetisation M_0 can be achieved by introducing an additional magnetic field, B_1. This energy, known as the excitation pulse (rf, radiofrequency energy), has to be applied with the same frequency as the Larmor frequency (resonance condition). The excitation of the spins system is the process of the energy absorption and results in the magnetisation moving from the z-axis to the transverse xy-plane, perpendicular to the direction of the main magnetic field.

During the pulse, the net external magnetic field will be the sum of $B_0 + B_1$. When all the magnetisation lies on the transverse plane, the resulting magnetisation will be called M_{xy} [1–3, 11].

When the rf pulse stops, immediately the protons will start to emit the energy absorbed. If nothing affects the homogeneity of the magnetic fields, all protons will rotate at the same resonance frequency. The portion of the magnetisation vector that is tilted towards the xy-plane, determines the initial amplitude of the signal. The maximum of the signal will be achieved when the angle is 90º; in that case the rf field will be called a 90º pulse.

The voltage in a receiving coil, located through the transverse plane, is the Magnetic Resonance signal, which will be collected and processed to generate the MRI [1–3].

The Free Induction Decay (FID) is originated by the rate of change of the magnetic flux and it is the voltage measured in the coil, according to Faraday's induction law:

$$\varepsilon = -\frac{d\Phi_B}{dt}, \tag{2.8}$$

being ε the electromotive force (EMF) and Φ_B the magnetic flux. This FID decays with time as the protons give up their absorbed energy through a process known as relaxation.

Two different processes take place during relaxation [2, 3, 10]:

- longitudinal relaxation: due to the recovery of the longitudinal magnetisation. This exchange of energy occurs between the spins and their surroundings (lattice) rather than to another spin, restoring thermal equilibrium. The spins go from a high energy state to a lower energy state, giving back the energy to the surrounding lattice. The longitudinal recovery follows an exponential curve, with a recovery rate represented by the time constant T_1.

- transversal relaxation: describing the decay of the transversal magnetisation. It corresponds to the spins being out of phase, when the corresponding magnetic fields interact, modifying slowly the precession rate. These interactions are temporal and random. This spin-spin relaxation causes a cumulative phase loss resulting in a decay of the transversal component of the magnetisation. The decay follows an exponential curve and it is characterised by the time constant T_2. T_1 relaxation is simultaneous to T_2; both occur at the same time, but with different mechanisms. However, the transversal relaxation is faster than the longitudinal one, thus $T_2 \ll T_1$.

Moreover, due to the field inhomogeneities, the transversal magnetisation decays faster, with a time constant T_2^*, then

$$\frac{1}{T_2^*} = \frac{1}{T_2} + \frac{1}{T_2'}, \tag{2.9}$$

where T_2' indicates the relaxation time due to inhomogeneities unrelated to the spins. By using an additional pulse the spins can be re-phased and the signal recovered. This signal will be the echo, and it will be the key of the next section.

2.3 Pulse sequences. Spin Echo

A pulse sequence is required to refocus the spins, to generate enough signal, hence, to produce at the end the desired image. Thus far, only the case of an application of a 90º pulse causing a FID has been described. Nonetheless, there is an enormous set of pulse sequences accessible for MRI.

In all pulse sequences three phases have to be considered [2, 3, 10, 12]:

- Preparation pulse to excite the spins system. The way this pulse is applied and the length of the flip angle have a significant impact in the parameter T_1.

- A time interval between the excitation and the data acquisition.

- A total time for the data sampling, T_R, or repetition time between two excitation pulses.

The proposal of the sequence spin echo in the 1950s by Hahn [13] was a powerful method and a key milestone in the field of magnetic resonance [2, 3, 5, 6, 11].

Even though spin echo is a slow sequence (in comparison with, for example, a gradient echo, where a gradient is employed to re-phase), is less susceptible to field inhomogeneities (T_2 decay instead of T_2^* as in gradient echo).

The sequence is described as follows:

The spins rotate along the $z-$direction. A rf pulse is applied at 90° (B_1), bringing down the magnetisation over the $xy-$plane. As some field inhomogeneities are always present, some spins precess faster than others, and the de-phasing occurs. At a time half of the echo time $\tau = \frac{T_E}{2}$ (T_E or echo time is the interval between the application of the excitation pulse and the signal collection), another 180° pulse is applied, allowing the recovery of phase coherence, and the generation of an echo at a time T_E after the pulse at 90°. The pulse at 180° serves to eliminate the effects of any static field inhomogeneities. Fig. 2.3 below illustrates the complete spin echo process:

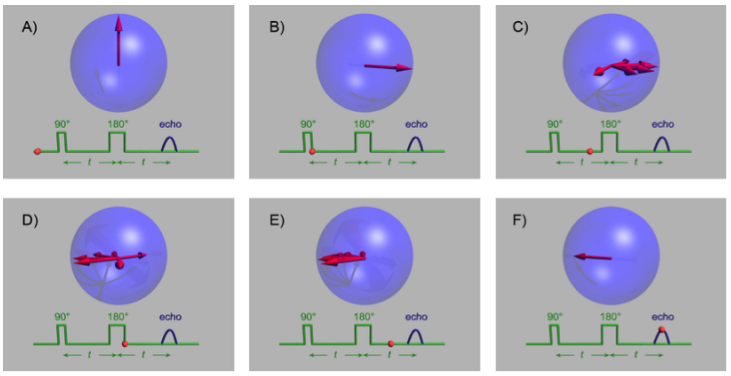

FIGURE 2.3: Spin echo sequence. [Source: http://www.wikipedia.org]

Other techniques of producing spin echo [14] were soon proposed after Hahn's paper.

There are also standard multiecho sequences, with multiple 180° rf pulses following a single excitation pulse. Although this kind of method could be useful in several fields, or depending on the desirable output image, in this project the focus relies on the standard single pulse echo.

2.3.1 Spin echo in other fields of physics

In quantum optics, the spin echo technique is widely exploited nowadays in experiments. In this field, the pulse sequence is applied to the Bloch vector, used to represent the density matrix. The density matrix formalism is useful to describe an ensemble of atoms [15].

In low temperature physics, NMR and MRI have been used to measure spatial distribution as an alternative to optical imaging methods [4].

2.4 Bose Einstein Condensation

A particular atomic isotope is bosonic or fermionic depending on the number of its constituents: protons, neutrons and electrons, being a boson (with integer total spin) if this number is even; or a fermion (with half-integer total spin) if it is odd.

S. Bose and A. Einstein first predicted the concept of Bose-Einstein condensation in the 1920s developing a statistical theory for an ideal gas of indistinguishable bosons. It was not until 1995 that C. Wieman, E. Cornell, and W. Ketterle did produce the first gaseous condensate of rubidium atoms cooled to 170 nanokelvin (see Fig. 2.4), receiving the 2001 Nobel Prize in Physics. This experience opened a new platform to realise experiments at very low temperatures [9].

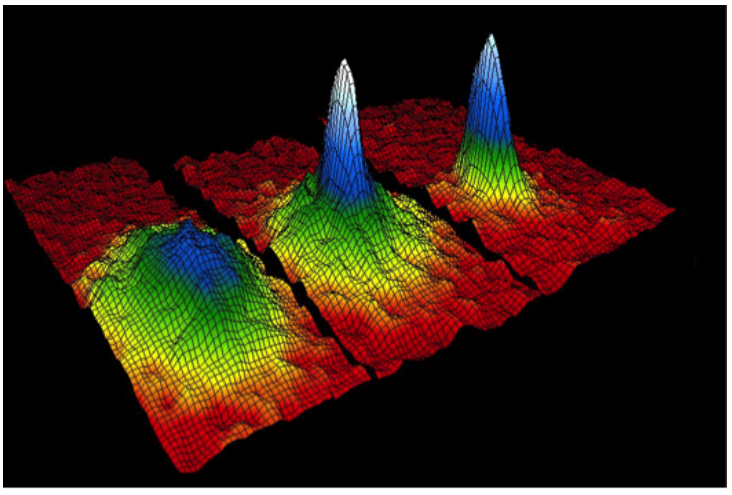

FIGURE 2.4: Bose-Einstein Condensation of ~ 2000 atoms of Rb at 200, 100, and ~ 20 nano-Kelvins. [Source: http://www.colorado.edu]

A Bose–Einstein condensate (BEC) is a state of matter of a dilute gas of bosonic particles cooled down to temperatures very close to absolute zero. Below this temperature, the de Broglie wavelengths of individual atoms become comparable to the size of the cloud and their wave functions start to overlap, giving rise to quantum coherence phenomena in the gas (every particle shares the same quantum wave function and phase). Under such conditions, a large fraction of bosons occupy the lowest quantum state, which means, the macroscopic occupation of a single-particle state [9].

In order to understand what was presented above, there are here below some useful definitions:

- The de Broglie wavelength is the wavelength, λ, associated with a particle, and related to its momentum, p, through the Planck constant, h: $\lambda = h/p$.

- A dilute gas is a gas with a low density, where the molecules barely interact; therefore, the probability of collision between more than two particles is negligible. The de Broglie length is much more smaller than the average separation between the molecules.

- The wave function in quantum mechanics describes the quantum state (description of the physical state that a physical system possesses at a given time in the frame of quantum mechanics) of an isolated system of one or more particles. The temporal evolution of the wave function is described by the Schrödinger equation (the equivalent in quantum mechanics of the Newtons's Second Law for classical physics) [8].

The single-particle wavefunction in a Bose–Einstein condensate is described using the Gross-Pitaevskii equation, which will be the main subject of the next chapter.

2.4.1 Rubidium

In this section some properties of the Rubidium will be presented, as ^{87}Rb has been chosen as the atomic species to be simulated in this project, not only because it was taken for the first BEC created in the lab, but also following the papers of Yasinaga and Tsubota [5, 6].

Table 2.3 shows the proton number Z, the neutron number N, the nuclear spin I, the nuclear magnetic moment μ, and the hyperfine splitting $\nu_{hf} = \Delta E_{hf}/h$ for hydrogen and some alkali isotopes (the hyperfine interaction couples the nuclear spin to the electronic spin).

The atomic spin is given by $F = I + J$, as explained in the Sec. 2.1.

In the electronic structure of alkali atoms all electrons but one occupy closed shells, and the remaining one is in an s orbital in a higher shell.

For Rubidium and all other alkali atoms in the electronic ground state $L = 0$, since the electrons have no orbital angular momentum. The coupling of the electronic spin is $S = 1/2$. Hence, $J = S = 1/2$ since $J = L + S$. The coupling of the electronic spin to the nuclear spin gives 2 possibilities: $F = I \pm 1/2$. The nuclear spin of ^{87}Rb is $I = 3/2$, resulting in $F_{upper} = 2$ and $F_{lower} = 1$. The energy difference between these two states, the ground hyperfine splitting, is 6.835 GHz [9].

Isotope	Z	N	I	μ/μ_N	ν_{hf} (MHz)
^{1}H	1	0	1/2	2.793	1420
^{6}Li	3	3	1	0.822	228
^{7}Li	3	4	3/2	3.256	804
^{23}Na	11	12	3/2	2.218	1772
^{39}K	19	20	3/2	0.391	462
^{40}K	19	21	4	−1.298	−1286
^{41}K	19	22	3/2	0.215	254
^{85}Rb	37	48	5/2	1.353	3036
^{87}Rb	37	50	3/2	2.751	6835
^{133}Cs	55	78	7/2	2.579	9193

TABLE 2.3: N, Z and the nuclear spin I for some alkali atoms and hydrogen. Source: [9]

These parameters are essential to attain experiments and theoretical simulations.

In the next chapter the mathematical introduction to the Gross-Pitaevskii equation for spinor Bose-Einstein condensates, and the election of the parameters used during the simulations will be presented.

Part III

Methodology

Chapter 3

The Gross-Pitaevskii equation

In this chapter, I highlight the mathematical formulation used to describe a Bose-Einstein condensate, using a non linear Schrödinger equation represented by the Gross-Pitaevskii equation. In Sec. 3.1, I present the basis to scattering theory. The general Gross-Pitaevskii equation is introduced in Sec. 3.2.

In Sec. 3.3 I define a spinor Bose-Einstein condensate. Finally, in Sec. 3.4, I discuss in more detail the 2-dimensional spin-1 Gross-Pitaevskii equation, which I will use later in the following chapters.

3.1 Basic scattering theory

In a Bose-Einstein condensate (BEC) the interactions between atoms are not negligible, and are indeed very important for the physics of these systems [9, 16, 17].

To describe scattering, the wave function for the relative motion is written as the sum of an incoming plane wave with definite angular momentum quantum number and a scattered wave. For low energy scattering, only the first few l-quantum numbers are affected. If all but the first term are discarded, only the s-waves take part in the scattering process. This is an approximation applied in the scattering of the atoms in a BEC. That is why at very low energies it is sufficient to consider s-wave scattering, and the wave function will take the form of [9]

$$\psi = 1 - \frac{a}{r}, \tag{3.1}$$

being r the vector separation of the two atoms and the constant a the scattering length.

In order to avoid short-term correlations when the wave function for many body systems is calculated, the concept of effective interaction is introduced. It describes the interaction between *long wavelengths, low frequency degrees of freedom of a system when coupling of these degrees of freedom via interactions with those at shorter wavelengths has been taken into account* [9]. It is used to calculate energies and is always proportional to the scattering length.

While the scattering lengths for alkali atoms are large compared with atomic dimensions, they are usually small compared with atomic separations in gas clouds. In very dilute systems, like quantum gases, the scattering length is much less than the inter-atomic spacing, and most of their properties are governed by the interaction between particles. Since in the ultra-cold regime only s-wave scattering between particles can take place, this allows one to replace the real inter-atomic potential (which at long distances is the usual van der Waals interaction) by a pseudo-potential, which is short range, isotropic and characterized by the s-wave scattering length a [9, 16, 17].

3.2 Introduction to the Gross-Pitaevskii equation

In order to understand the formulation it is necessary to review the standard time dependant Schrödinger equation,

$$i\hbar\frac{\partial}{\partial t}\Psi = \hat{H}\Psi, \tag{3.2}$$

with Ψ the wave function of the quantum system, and $\hat{H}$ the Hamiltonian operator. For a non-relativistic particle

$$i\hbar\frac{\partial}{\partial t}\psi(\mathbf{r},t) = \left[-\frac{\hbar^2}{2m}\nabla^2 + V(\mathbf{r})\right]\psi(\mathbf{r},t). \tag{3.3}$$

where V is the potential energy, ∇^2 is the Laplacian (a differential operator), and ψ is the wave function (the "position-space wave function").

Generally, the Hamiltonian describes the total energy of any given wave function, and taking the analogy with classical mechanics, the total energy will contain kinetic energy plus potential energy.

Analogously, a Bose-Einstein condensate can be described by the following Hamiltonian [9, 17, 18]:

$$\hat{H} = \sum_{i=1}^{N} \frac{\hbar^2}{2m} \nabla^2 + \sum_{i=1}^{N} V_{ext}(\mathbf{r}_i) + \sum_{i<j} U(\mathbf{r}_i, \mathbf{r}_j), \tag{3.4}$$

with N the number of particles, V_{ext} is the one body external potential, and U a two-body interaction potential.

To derive the Hamiltonian in the mean field theory, applying second quantisation, the Many-Body-Hamiltonian is described using the following equation:

$$\hat{H} = \int dr \hat{\Psi}^\dagger(\mathbf{r}) \left[-\frac{\hbar^2}{2m} \nabla^2 + V_{ext} \right] \hat{\Psi}(\mathbf{r}) + \frac{1}{2} \int dr dr' \hat{\Psi}^\dagger(\mathbf{r}) \hat{\Psi}^\dagger(\mathbf{r'}) U(\mathbf{r} - \mathbf{r'}) \hat{\Psi}(\mathbf{r'}) \hat{\Psi}(\mathbf{r}), \tag{3.5}$$

with $U(\mathbf{r} - \mathbf{r}')$ the two body interaction potential, and Ψ the field operator that satisfies the following relation:

$$\left[\Psi(\mathbf{r'}, t), \Psi^\dagger(\mathbf{r}, t) \right] = \Delta(\mathbf{r} - \mathbf{r}'). \tag{3.6}$$

where the Heisenberg picture version of the Schrödinger equation is given by

$$i\hbar \frac{\partial}{\partial t} \hat{\Psi}(\mathbf{r}, t) = \left[\hat{\Psi}(\mathbf{r}, t), \hat{H} \right]. \tag{3.7}$$

The Many-Body-Hamiltonian in the standard time dependant Schrödinger equation will then become:

$$i\hbar \frac{\partial}{\partial t} \hat{\Psi}(\mathbf{r}, t) = \left[-\frac{\hbar^2}{2m} \nabla^2 + V_{ext}(\mathbf{r}) + \int dr' \hat{\Psi}^\dagger(\mathbf{r}', t) U(\mathbf{r} - \mathbf{r}') \hat{\Psi}(\mathbf{r}', t) \right] \hat{\Psi}(\mathbf{r}, t). \tag{3.8}$$

Applying the Bogoliubov approximation (the condensate wave function is approximated by a sum of the equilibrium wave function and a small perturbation):

$$\hat{\Psi}(\mathbf{r}, t) = \Phi(\mathbf{r}, t) + \hat{\Psi}'(\mathbf{r}, t), \tag{3.9}$$

with

$$\Phi(\mathbf{r}, t) = \langle \hat{\Psi}(\mathbf{r}, t) \rangle \tag{3.10}$$

the field mean value or the condensate wavefunction, and $\hat{\Psi}'$ represents the non condensed fraction.

As reviewed in Eq. 3.1, the s-wave contribution dominates the scattering of a pair of particles and it is described by the scattering length. Introducing the limit where the

contact potential is a delta function (Born approximation in the pseudopotential, see [19]):

$$U(\mathbf{r}-\mathbf{r}') = g\delta(\mathbf{r}-\mathbf{r}'), \tag{3.11}$$

where

$$g = \frac{4\pi\hbar^2 a}{m}, \tag{3.12}$$

then the Gross-Pitaevskii equation form can be deduced:

$$i\hbar\frac{\partial}{\partial t}\Phi(\mathbf{r},t) = \left[-\frac{\hbar^2}{2m}\nabla^2 + V_{ext}(\mathbf{r}) + g \mid \Phi(\mathbf{r},t) \mid^2\right]\Phi(\mathbf{r},t). \tag{3.13}$$

Starting from the Hamiltonian in second quantisation, the Heisenberg equation of motion (Eq. 3.7) can be derived. Then by replacing the quantum field operator with a classical field we obtain:

$$\hat{\Psi} \rightarrow \psi(\mathbf{r},t) \approx \sqrt{N}\Phi(\mathbf{r},t), \tag{3.14}$$

with N the number of atoms present in the BEC.

In this case there are many atoms in one quantum state, and the fluctuations on the single atom level are neglected.

Replacing directly the field operator with the classical condensate function, Equation 3.15 is obtained:

$$i\hbar\frac{\partial}{\partial t}\psi(\mathbf{r},t) = \left[-\frac{\hbar^2}{2m}\nabla^2 + V_{ext}(\mathbf{r}) + g \mid \psi(\mathbf{r},t) \mid^2\right]\psi(\mathbf{r},t). \tag{3.15}$$

It is important to notice that the condensate wave function represents the classical limit of the de Broglie waves for the atoms, the existence of individual atoms is no longer important.

The general time-dependant Gross-Pitaevskii (GP) equation (Eq. 3.15), developed by E. Gross and L. Pitaevskii in 1961, describes the zero-temperature properties of the non-uniform Bose gas when the scattering length a is much less than the mean interparticle spacing [9, 16, 17], and it is the basis for the equation to be employed during the simulations.

3.3 Spinor BEC

Spinor condensates are BEC with internal spin degrees of freedom, offering complex internal quantum features and rich in quantum dynamics, due to the vector properties of the condensate order parameter and the nonlinear spin-spin interactions. To be able to observe these spinor condensates, special techniques for trapping have been developed, like optical traps where the gas is trapped with lasers, and the spin of the atoms is free, make possible to have all spin states occupied. In optical traps the potential is independent of the hyperfine state, and it is posible to investigate the dynamics of the spin [9, 16, 20–22].

As it was explained in Sec. 2.4.1, the ground hyperfine splitting is the difference between the two states $F_{upper} = 2$ and $F_{lower} = 1$. In a BEC when the atoms approach each other, a total spin will be formed from a temporal coupling of the individual spins, and the atomic spins precess around this total spin during the collision. After the collision, the two spins decouple and the atoms separate from each other.

Table 3.1 shows some experimental candidates for the study of ultracold spinor Bose gases. In brackets the nature of the spin dependent contact (f: ferromagnetic, af: antiferromagnetic, cyc: cyclic or tetrahedral, ?: unknown) is indicated.

Stable		Unstable
$\langle F_z \rangle$ conserved	$\langle F_z \rangle$ not conserved	
^{7}Li, $F = 1$ (f)	^{52}Cr, $F = 3$ (not f)	^{7}Li, $F = 2$
^{23}Na, $F = 1$ (af)	Dy, $F = 8$ (?)	^{23}Na, $F = 2$
^{41}K, $F = 1$ (f)	Er, $F = 6$ (?)	^{39}K
^{87}Rb, $F = 1$ (f)		^{85}Rb
^{87}Rb, $F = 2$ (af or cyc)		^{133}Cs
^{87}Rb pseudospin:	Tm, $F = 4$ (?)	
$\|1, 0\rangle$, $\|2, 0\rangle$		
$\|1, \pm 1\rangle$, $\|2, \mp 1\rangle$		

TABLE 3.1: Experimental candidates for the study of ultracold spinor Bose gases. Source: [23]

The total spin for two identical spin-f particles will be $F = f_1 + f_2$, where the total spin allowed are $F = 2f, 2f - 1, ..., 0$. Due to the symmetry required by identical bosons, as it is the case in this thesis, only even channels for F are allowed. Since the focus here is on spin-1 condensates, the allowed collision channels are $F = 0, 2$. Therefore the s-wave scattering lengths $a_{F=0}$ and $a_{F=2}$ are the two parameters required to describe the interactions. From now on $a_{F=0} = a_0$ and $a_{F=2} = a_2$ will be utilised [16, 23].

The general form of the interaction will have the contribution of the different total spin channels, in this case:

$$U(\mathbf{r}_1 - \mathbf{r}_2) = \delta(\mathbf{r}_1 - \mathbf{r}_2)(g_0 P_0 + g_2 P_2), \tag{3.16}$$

where P_F is a projector operator which projects the pair of atoms into a total hyperfine spin F state, with respectively:

$$P_0 = \frac{1 - \mathbf{S}_1\mathbf{S}_2}{3} \tag{3.17}$$

and

$$P_2 = \frac{2 + \mathbf{S}_1\mathbf{S}_2}{3}, \tag{3.18}$$

as the product of the spin operators is

$$\mathbf{S}_1\mathbf{S}_2 = P_2 - 2P_0. \tag{3.19}$$

Hence, the contact interaction can be written as:

$$g_0 P_0 + g_2 P_2 = c_0 + c_2 \mathbf{S}_1\mathbf{S}_2, \tag{3.20}$$

where

$$c_0 = \frac{g_0 + 2g_2}{3} \tag{3.21}$$

and

$$c_2 = \frac{g_2 - g_0}{3}, \tag{3.22}$$

being c_0 the interaction constant between atoms and c_2 the spin exchange interaction constant [9, 23, 24], that can be written as well as:

$$c_0 = \frac{4\pi\hbar^2}{m}\overline{a} \tag{3.23}$$

and

$$c_2 = \frac{4\pi\hbar^2}{m}\frac{\Delta a}{3}, \tag{3.24}$$

being the coupling:

$$g_F = \frac{4\pi\hbar^2 a_F}{m}. \tag{3.25}$$

The expression

$$\overline{a} = \frac{(a_0 + 2a_2)}{3} \tag{3.26}$$

is the mean s-wave scattering length and $\Delta a = a_2 - a_0$ is the scattering length difference.

3.4 Spin-1 condensate GP equation

As described before, in each F state, there are $2F+1$ Zeeman sublevels denominated $m_F = F, F-1, \ldots, -F$, and in this case where $F=1$, m can take values of 1,0, and -1. Instead of choosing the basis $|1\rangle$, $|0\rangle$ and $|-1\rangle$, a new basis is introduced: $S_i|i\rangle = 0$ with $i = x, y, z$ where S_i is the $i-th$ component of the spin operator. In the following notation, the sub-index α indicates the specific state.

The Hamiltonian for the $F=1$ spinor BEC for a many-body system with the effective interaction in second quantisation is then defined as [9, 20, 24–27]:

$$\hat{H} = \int \left[-\frac{\hbar^2}{2m}\nabla\psi_\alpha^*\nabla\psi_\alpha + V(\mathbf{r})\psi_\alpha^*\psi_\alpha - g\mu_B\psi_\alpha^*\mathbf{B}_i\mathbf{S}_{\alpha\beta}^i\Psi_\beta + \frac{1}{2}c_0\psi_\alpha^*\psi_{\alpha'}^*\psi_{\alpha'}\psi_\alpha + \frac{1}{2}c_2\psi_\alpha^*\psi_{\alpha'}\mathbf{S}_{\alpha\beta}\mathbf{S}_{\alpha'\beta'}\psi_{\beta'}\psi_\beta \right] d\mathbf{r} \tag{3.27}$$

with the additional term $g\mu_B\psi_\alpha^\dagger\mathbf{B}_i\mathbf{S}_{\alpha\beta}^i\psi_\beta$ indicating the presence of a gradient or magnetic field term($\mathbf{B}$), with g the Lande $g-$factor and μ_B the Bohr magneton. ψ^* represents the conjugate of ψ.

The Pauli matrices are represented by $S_{\alpha\beta}^i$ with $i = x, y, z$:

$$S_{\alpha\beta}^x = \frac{1}{\sqrt{2}}\begin{bmatrix} 0 & 1 & 0 \\ 1 & 0 & 1 \\ 0 & 1 & 0 \end{bmatrix}; \tag{3.28}$$

$$S_{\alpha\beta}^y = \frac{1}{\sqrt{2}}\begin{bmatrix} 0 & -i & 0 \\ i & 0 & -i \\ 0 & i & 0 \end{bmatrix}; \tag{3.29}$$

$$S_{\alpha\beta}^z = \begin{bmatrix} 1 & 0 & 0 \\ 0 & 0 & 0 \\ 0 & 0 & -1 \end{bmatrix} \tag{3.30}$$

Being $\mathbf{S} = S_x\bar{i} + S_y\bar{j} + S_z\bar{k}$, the component of the spin density vector is given by:

$$\mathbf{S}_i = \sum_{\alpha,\beta}\psi_\alpha^*\mathbf{S}_{\alpha\beta}^i\psi_\beta, \tag{3.31}$$

where each component will be represented as [9, 28]:

$$S_x = \frac{1}{\sqrt{2}}\left[\psi_1^*\psi_0 + \psi_0^*(\psi_1 + \psi_{-1}) + \psi_{-1}^*\psi_0\right] \tag{3.32}$$

$$S_y = \frac{i}{\sqrt{2}}\left[-\psi_1^*\psi_0 + \psi_0^*(\psi_1 - \psi_{-1}) + \psi_{-1}^*\psi_0\right] \tag{3.33}$$

$$S_z = |\psi_1|^2 - |\psi_{-1}|^2, \tag{3.34}$$

being ψ_1, ψ_0 and ψ_{-1} the three components of the wavefunction.

Ultimately, following the standard procedure in the mean-field description, the spin-1 Gross-Pitaevskii (GP) equation will take the form [5, 6, 27]:

$$i\hbar\frac{\partial}{\partial t}\psi_\alpha = \left[-\frac{\hbar^2}{2m}\nabla^2 + V\right]\psi_\alpha - g\mu_B\mathbf{B}_i\mathbf{S}^i_{\alpha\beta}\Psi_\beta + \frac{1}{2}c_0\psi^*_\beta\psi_\beta\psi_\alpha + \frac{1}{2}c_2\mathbf{S}_i\mathbf{S}^i_{\alpha\beta}\psi_\beta. \tag{3.35}$$

The previous equation is the basis for the simulations to be done in this project. In the next section the value of the different parameters selected will be introduced.

In the following chapters the simulation of the Gross-Pitaevskii will be computed and the results presented.

Part IV

Results and discussion

Chapter 4

Equation simulation

In this chapter the numerical package that have been employed during the project to simulate the two-dimensional spin-1 Gross-Pitaevskii equation (GPE) for a spinor BEC is described, namely GPELab. Sec. 4.1 introduces the general environment to compute stationary states and dynamics for a GPE. In Sec. 4.2 the utilisation of this tool for the spin-1 case presented in the previous chapter is detailed.

The systems in this project are quantum, and nowadays it is technically extremely complex and expensive to perform an experiment in order to observe the physical phenomena at the quantum level. By using numerical simulations it is possible to experiment complex configurations in a cheaper way.

4.1 General GPE in the environment of GPELab

Firstly, in order to understand how the simulation has been done, it is necessary an introduction to the general environment of GPELab [29].

GPELab has been selected the tool to be used during the simulations because it offers excellent conditions to compute stationary as well as dynamical behaviour of non linear Schrödinger equations, that is, Gross-Pitaevskii equations. The toolbox is based on recent and updated numerical methods and it is written in $MATLAB^{®}$, making it exceptionally helpful when using the program.

Eq. 3.15 obtained in Chapter 3 will be the basis of the following derivation. The equation is given by:

$$i\hbar\frac{\partial}{\partial t}\psi(\mathbf{r},t) = \left[-\frac{\hbar^2}{2m}\nabla^2 + V_{ext}(\mathbf{r}) + g \mid \psi(\mathbf{r},t) \mid^2\right]\psi(\mathbf{r},t). \tag{4.1}$$

Considering the following changes of variables:

- $t \longrightarrow \frac{t}{\omega}$.
- $\psi \longrightarrow \frac{\psi}{a_0^{\frac{3}{2}}}$. with

$$a_0 = \sqrt{\frac{\hbar}{m\omega}}. \tag{4.2}$$

Now taking a term representing the non-linearity strength which describes the interactions between atoms in the condensate defined as

$$\beta = \frac{4\pi a N}{a_0}, \tag{4.3}$$

the equation can be reduced to:

$$i\hbar\frac{\partial}{\partial t}\psi = \left[-\frac{1}{2m}\nabla^2 + V_d + \beta_d \mid \psi \mid^2\right]\psi, \tag{4.4}$$

with d the dimension of the problem and N the number of atoms in the condensate. This step is necessary to show the resulting equation which will be simulated by the numerical methods.

Eq. 4.4 characterises the basic GPE to be solved and, by adding supplementary terms, a specific problem can be defined.

4.1.1 Stationary states

For the purpose of computing a stationary state, like the ground state, it is necessary to find the numerical solution to the equation given. Eq. 4.4 can be rewritten in a more general way as:

$$i\hbar\frac{\partial}{\partial t}\psi(t,\mathbf{r}) = \hat{H}\left(\mathbf{r}, -i\nabla^2\right)\psi(t,\mathbf{r}). \tag{4.5}$$

The stationary states are the eigenfunctions of the operator $\hat{H}$. Then, for each eigenfunction, we have

$$\hat{H}\left(\mathbf{r}, -i\nabla^2\right)\phi(\mathbf{r}) = \mu\phi(\mathbf{r}), \tag{4.6}$$

where μ is the associated eigenvalue.

That is, for a time dependent GPE a solution is given by

$$\psi(t, \mathbf{r}) = e^{-i\mu t}\phi(\mathbf{r}), \tag{4.7}$$

with $\phi(\mathbf{r})$ a time independent function.

ϕ must be normalised:

$$\int_{\mathbb{R}^2} |\phi(\mathbf{r})|^2 d\mathbf{r} = 1, \tag{4.8}$$

In order to solve numerically the equation, an iteration method is needed.

In GPELab the imaginary time method is used, and the critical points are searched by a Continuous Normalized Gradient Flow (CNGF) (for additonal information please refer to [29–31]). This method consists in:

- a gradient flow on a certain time interval,
- a projection on the constraint manifold.

To further discretise the equation, time and space discretisation have to be considered.

4.1.1.1 Numerical Methods for time discretisation

Here I give a general introduction to the basis of the numerical methods used for time discretisation. The time step is the key parameter to be introduced when using an iterative method, and from now it is defined as Δt.

Using the notation of the n-th time step as t^n with a solution given by ϕ^n, an ordinary differential equation is defined by:

$$\frac{d\phi}{dt} = f(t, \phi), \tag{4.9}$$

with $f(t, \phi)$ an arbitrary function and initial conditions $\phi(t^0) = \phi^0$.

The two methods generally employed to solve these kind of equations are:

1. Backward Euler [32]

Taking Eq. 4.9 and applying:

$$\frac{\phi^n - \phi^{n-1}}{\Delta t} = f(t^n, \phi^n), \tag{4.10}$$

then,

$$\phi^n = \phi^{n-1} + \Delta t f(t^n, \phi^n). \tag{4.11}$$

Next, by stepping the index n to $n+1$, the equation for the implicit method of Backwards Euler is obtained:

$$\phi^{n+1} = \phi^n + \Delta t f(t^{n+1}, \phi^{n+1}), \tag{4.12}$$

2. Crank-Nicholson [33]

The equation for the Crank-Nicholson method can be found as:

$$\frac{\phi^{n+1} - \phi^n}{\Delta t} = \frac{1}{2} f(t^{n+1}, \phi^{n+1}) + \frac{1}{2} f(t^n, \phi^n), \tag{4.13}$$

and rearranging the terms, the following equation is obtained:

$$\phi^{n+1} = \phi^n + \frac{\Delta t}{2} \left[f(t^{n+1}, \phi^{n+1}) + f(t^n, \phi^n) \right]. \tag{4.14}$$

The time discretisation method to be applied will depend on the type of problem to be computed.

4.1.1.2 Numerical Methods for space discretisation

Spatial discretisation provides the use of a spatial grid, where only a discrete set of values of ϕ is defined.

GPELab considers an approach based on Fourier series representations through Fast Fourier Transforms (FFTs).

For more information to deepen into the calculation of these stationary states for the general GPE please relate to [29–31].

4.1.2 Dynamics

In this project the interest focusses on the dynamical simulations, rather than on finding the stationary states. Therefore, the details of the numerical method used for the dynamics will be presented in this section.

The scheme that is employed (and that needs to be utilised in most of the dynamical simulation) is a relaxation scheme (Crank-Nicholson with a relaxed non-linearity).

4.1.2.1 The relaxation scheme

This scheme was introduced by Besse [34] and it is based in the Crank-Nicholson without solving a non-linear equation (through a fixed point or a Newton-Raphson method).

First of all, the method is based on the the Crank-Nicholson since this is the only approach conserving both density and energy.

The procedure applied to Eq. 4.4 with $\hbar = m = 1$ is given by:

$$\begin{cases} \frac{\phi^{n+1/2}+\phi^{n-1/2}}{2} = \beta|\psi^n|^2 \\ i\frac{\psi^{n+1}+\psi^n}{\delta t} = \left(-\frac{1}{2}\nabla^2 + \phi^{n+1/2}\right)\left(\frac{\psi^{n+1}+\psi^n}{2}\right) + \frac{V^{n+1}\psi^{n+1}+V^n\psi^n}{2}, \end{cases} \tag{4.15}$$

with $\phi^{n+1/2} = \phi(t_{n+1/2}, \mathbf{r})$, $\psi^n = \psi(t_n, \mathbf{r})$, $V^n = V(t_n, \mathbf{r})$, and with initial conditions: $\psi^0 = \psi_0$ and $\phi^{-1/2} = \beta|\psi_0|^2$ [7, 34].

By applying the spatial discretisation using the pseudospectral method by Fourier expansion (instead of a finite difference scheme, pseudospectral approximation of the spatial derivatives can be used to get high-order accuracy [7]), the following system of equations is obtained:

$$\begin{cases} [\![\phi^{n+1/2}]\!] = 2\beta[\![\psi^n|^2]\!] - [\![\phi^{n-1/2}]\!] \\ \mathbb{A}^{Re,n}\psi^{n+1} = b^{Re,n}, \end{cases} \tag{4.16}$$

where the operator $\mathbb{A}^{Re,n}$ is given by:

$$\mathbb{A}^{Re,n} := \left(i\frac{[\![I]\!]}{\delta t} + \frac{1}{4}[\![\nabla^2]\!] - \frac{1}{2}[\![V^{n+1}]\!] - \frac{1}{2}[\![[\phi^{n+1/2}]\!]\right), \tag{4.17}$$

and the vector $b^{Re,n}$

$$b^{Re,n} := \left(i\frac{[\![I]\!]}{\delta t} - \frac{1}{4}[\![\nabla^2]\!] + \frac{1}{2}[\![V^n]\!] + \frac{1}{2}[\![\phi^{n+1/2}]\!]\right)\psi^n. \tag{4.18}$$

These equations are the basis for the relaxation scheme applied in any dynamical simulation using the toolbox GPELab.

Further clarification and details can be found in [7, 29, 34].

4.2 Spin-1 GPE for a spinor BEC in the environment of GPELab

In the previous section a general introduction to the methodology followed by GPELab has been given. Nevertheless, all the examples have been simple GPEs, whereas the interest of this project is related to the dynamical simulations of the GPE for spin-1 spinor BECs.

The first step is to characterise the multicomponent case, that is, when there is a system of coupled Gross-Pitaevskii equations.

4.2.1 N-components

Eq. 4.4 in the multicomponent case will take the form [29, 31, 35]:

$$i\hbar\frac{\partial}{\partial t}\Psi(t,\mathbf{r}) = -\frac{1}{2}\nabla^2\Psi(t,\mathbf{r}) + V(\mathbf{r})\Psi(t,\mathbf{r}) + \beta F(\Psi(t,\mathbf{r}),\mathbf{r})\Psi(t,\mathbf{r}), \tag{4.19}$$

with $\Psi = (\psi_1, ..., \psi_N)$, $F(\Psi(t,\mathbf{r})$ the non linearity matrix, and the initial conditions $\Psi(t=0,\mathbf{r}) := \Psi_0(\mathbf{r})$.

The solution to the stationary state will have the form:

$$\Psi(t,\mathbf{r}) = e^{-i\mu t\Phi(\mathbf{r})}, \tag{4.20}$$

where $\Phi = (\phi_1, ..., \phi_N)$ is a time independent function.

Time and space discretisation are anew applied to the multicomponent case when the stationary state is calculated.

Regarding the dynamics of the system, the relaxation scheme can as well be extended when there is more than one component.

Eq. 4.15 will take the form [7, 29, 35]:

$$\begin{cases} \frac{\Phi^{n+1/2}+\Phi^{n-1/2}}{2} = \beta F \Psi^n \\ i\frac{\Psi^{n+1}+\Psi^n}{\delta t} = -i\left(\frac{1}{2}\nabla^2 + \Phi^{n+1/2}\right)\left(\frac{\Psi^{n+1}+\Psi^n}{2}\right) + \frac{V^{n+1}\Psi^{n+1}+V^n\Psi^n}{2}, \end{cases} \tag{4.21}$$

with

$$\begin{cases} [\![\Phi^{n+1/2}]\!] = 2\beta[\![F(\Psi^n)]\!] - [\![\Phi^{n-1/2}]\!] \\ \mathbb{A}^{Re,n}\Psi^{n+1} = B^{Re,n}. \end{cases} \tag{4.22}$$

The operator $\mathbb{A}^{Re,n}$ will result in:

$$\mathbb{A}^{Re,n} := \left(i\frac{[\![I]\!]}{\delta t} + \frac{1}{4}[\![\nabla^2]\!] - \frac{1}{2}[\![V^{n+1}]\!] - \frac{1}{2}[\![\Phi^{n+1/2}]\!]\right), \tag{4.23}$$

and the vector $b^{Re,n}$

$$b^{Re,n} := \left(i\frac{[\![I_N]\!]}{\delta t} - \frac{1}{4}[\![\nabla^2]\!] + \frac{1}{2}[\![V^n]\!] + \frac{1}{2}[\![\Phi^{n+1/2}]\!]\right)\psi^n. \tag{4.24}$$

Adopting the multi component form, the ingredients to represent the equation for a spin-1 GPE for a spinor BEC are already available.

4.2.2 Spin-1 GPE for a spinor BEC

The three couple equations will represent the Zeemann sublevels as described in Chapter 3.

The Hamiltonian for the $F = 1$ spinor BEC in second quantisation was defined equation in Eq. 3.27. The starting point will be the same equation without the magnetic field:

$$\hat{H} = \int \left[-\frac{\hbar^2}{2m}\nabla\psi^*_\alpha\nabla\psi_\alpha + V(\mathbf{r})\psi^*_\alpha\psi_\alpha + \frac{1}{2}c_0\psi^*_\alpha\psi^*_{\alpha'}\psi_{\alpha'}\psi_\alpha + \frac{1}{2}c_2\psi^*_\alpha\psi_{\alpha'}\mathbf{S}_{\alpha\beta}\mathbf{S}_{\alpha'\beta'}\psi_{\beta'}\psi_\beta\right] d\mathbf{r}, \tag{4.25}$$

and the three component wavefunction $\Psi(\mathbf{r},t) = (\psi_1(\mathbf{r},t), \psi_0(\mathbf{r},t), \psi_{-1}(\mathbf{r},t))^T$ are described by the coupled equations [36, 37]:

$$i\hbar\frac{\partial}{\partial t}\psi_1(\mathbf{r},t) = \left[-\frac{\hbar^2}{2m}\nabla^2 + V(\mathbf{r}) + (c_0+c_2)(|\psi_1|^2 + |\psi_0|^2) + (c_0-c_2)(|\psi_{-1}|^2\right]\psi_1 + c_2\psi^*_{-1}\psi_0^2, \tag{4.26}$$

$$i\hbar\frac{\partial}{\partial t}\psi_0(\mathbf{r},t) = \left[-\frac{\hbar^2}{2m}\nabla^2 + V(\mathbf{r}) + (c_0+c_2)(|\psi_1|^2 + |\psi_{-1}|^2) + c_0(|\psi_0|^2\right]\psi_0 + 2c_2\psi_{-1}\psi^*_0\psi_1, \tag{4.27}$$

$$i\hbar\frac{\partial}{\partial t}\psi_{-1}(\mathbf{r},t) = \left[-\frac{\hbar^2}{2m}\nabla^2 + V(\mathbf{r}) + (c_0+c_2)(|\psi_{-1}|^2+|\psi_0|^2) + (c_0-c_2)(|\psi_1|^2\right]\psi_{-1} + c_2\psi_0^2\psi_1^*. \tag{4.28}$$

Hence, using the change of variables like in Section 4.1, the coupled GPEs in d dimensions can be written as:

$$i\frac{\partial}{\partial t}\psi_1(\mathbf{r},t) = \left[-\frac{1}{2}\nabla^2 + V(\mathbf{r}) + (\beta_n+\beta_s)(|\psi_1|^2+|\psi_0|^2) + (\beta_n-\beta_s)(|\psi_{-1}|^2\right]\psi_1 + \beta_s\psi_{-1}^*\psi_0^2, \tag{4.29}$$

$$i\frac{\partial}{\partial t}\psi_0(\mathbf{r},t) = \left[-\frac{1}{2}\nabla^2 + V(\mathbf{r}) + (\beta_n+\beta_s)(|\psi_1|^2+|\psi_{-1}|^2) + \beta_n(|\psi_0|^2\right]\psi_0 + 2\beta_s\psi_{-1}\psi_0^*\psi_1, \tag{4.30}$$

$$i\frac{\partial}{\partial t}\psi_{-1}(\mathbf{r},t) = \left[-\frac{1}{2}\nabla^2 + V(\mathbf{r}) + (\beta_n+\beta_s)(|\psi_{-1}|^2+|\psi_0|^2) + ((\beta_n-\beta_s)(|\psi_1|^2\right]\psi_{-1} + \beta_s\psi_0^2\psi_1^*, \tag{4.31}$$

where

$$\beta_n = \frac{Nc_0}{a_0^3\hbar\omega}, \tag{4.32}$$

and

$$\beta_s = \frac{Nc_2}{a_0^3\hbar\omega}. \tag{4.33}$$

Eq. 4.29, Eq. 4.30 and Eq. 4.31 are the equations to be simulated to study the dynamics by applying a spin echo sequence.

The results representing the evolution of the spins with time will be presented in the next chapter .

Chapter 5

Spin evolution according equation results

As it has been described in Chapter 2, the spin echo technique can be used to explore the physics that is associated with a variety of models, making this technique a doubtless tool in a wide range of fields.

The purpose of this chapter is to analyse the behaviour of spin-echo applied to a spinor BEC, evaluating how the spin density vector evolves in time. Additionally, the stationary states with and without magnetic field are investigated.

The chapter is organized as follows: in Sec. 5.1, the general parameters for the case studied are set. In Sec. 5.2, the case of a spin-1 spinor without any magnetic field is investigated. The simulation is performed with the additional magnetic field in Sec. 5.3. Lastly, in the same section, the spin evolution under a spin echo pulse sequence is examined.

5.1 Election of parameters for the simulation

The specific Bose-Einstein condensate studied in this project is a ^{87}Rb BEC trapped by a harmonic potential of frequency ω.

The equation to be simulated is the two-dimensional spin-1 Gross-Pitaevskii (GP) equation for a spinor BEC, that is, the three coupled equations derived in the previous chapter:

$$i\frac{\partial}{\partial t}\psi_1(\mathbf{r},t) = \left[-\frac{1}{2}\nabla^2 + V(\mathbf{r}) + (\beta_n+\beta_s)(|\psi_1|^2+|\psi_0|^2) + (\beta_n-\beta_s)(|\psi_{-1}|^2\right]\psi_1 + \beta_s\psi_{-1}^*\psi_0^2, \tag{5.1}$$

$$i\frac{\partial}{\partial t}\psi_0(\mathbf{r},t) = \left[-\frac{1}{2}\nabla^2 + V(\mathbf{r}) + (\beta_n+\beta_s)(|\psi_1|^2+|\psi_{-1}|^2) + \beta_n(|\psi_0|^2\right]\psi_0 + 2\beta_s\psi_{-1}\psi_0^*\psi_1, \tag{5.2}$$

$$i\frac{\partial}{\partial t}\psi_{-1}(\mathbf{r},t) = \left[-\frac{1}{2}\nabla^2 + V(\mathbf{r}) + (\beta_n+\beta_s)(|\psi_{-1}|^2+|\psi_0|^2) + ((\beta_n-\beta_s)(|\psi_1|^2\right]\psi_{-1} + \beta_s\psi_0^2\psi_1^*, \tag{5.3}$$

The different parameters will be described next, together with the specific values set during the numerical simulations:

- $\hbar = 1$.

- $V = m\omega^2\frac{x^2+y^2}{2}$. For simplification during the numerical simulation m and ω have been set up to 1.

- $N = 10^4$, as a typical value of the number of atoms employed in these kind of experiments [38].

- For ^{87}Rb, $-c_2 \ll c_0$, with values of $c_2 = -3.1\cdot 10^{-10}$ and $c_0 = 6.70747\cdot 10^{-8}$, by using $a_0 = 101.8$ and $a_2 = 100.4$ (in terms of the Bohr radius $a_B = 5.2917720859\cdot 10^{-11}$) from [23], and with the corresponding substitution in Eq. 3.21 and Eq. 3.22.

Consequently, the calculation of β_n and β_s as defined in the previous chapter will result in $\beta_s = -3.1\cdot 10^{-6}$ and $\beta_n = 6.70747\cdot 10^{-4}$.

Once the variables have been specified, the simulations can be started.

NOTE1 $\Rightarrow$ all results will be shown as a projection on the $xy-$plane.

NOTE2 $\Rightarrow$ the following configuration was used for the simulations: CPU Intel Core i5 (1.3 GHz) CPU, Memory 4 Gb RAM, and the software was $MATLAB^{®}$ version R2015a.

5.2 Solution without any magnetic field

A substantial number of papers have been published focussed on finding the stationary solutions, mainly the ground state, of BECs [35, 39–41], as well as in spinors BECs, such as in [40, 41].

As discussed in Chapter 4, it is necessary to employ numerical tools to be able to solve these kind of non linear differential equations.

The details and results of this computation are described next.

5.2.1 Model computation for the stationary solution

In the simulation performed here, using GPELab, the solution is found with a BESP scheme (Backward Euler SPectral using Fast Fourier Transforms, see Chapter 4 for the background on these numerical methods).

The system of coupled equations is the one described by the Eqs. 5.1-5.3 with parameters defined as in the last section.

The time step chosen for the time discretisation has a value of $\Delta t = 0.1$ with a maximum of 10 iterations. The CPU time for this calculation was about 8.1 seconds.

Fig. 5.1 shows the modulus of the wavefunction for the solution of the ground state in the 3 components, respectively:

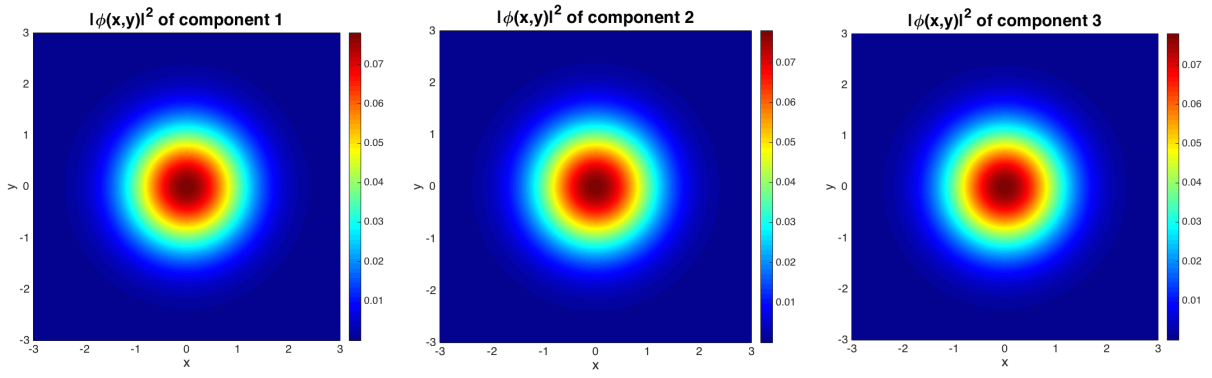

FIGURE 5.1: The 3 components of the ground state solution for the 2D spin-1 spinor ^{87}Rb BEC.

It is possible to observe that the three components are essentially identical.

As an additional result, Fig. 5.2 represents the Sx component of the spin in the ground state.

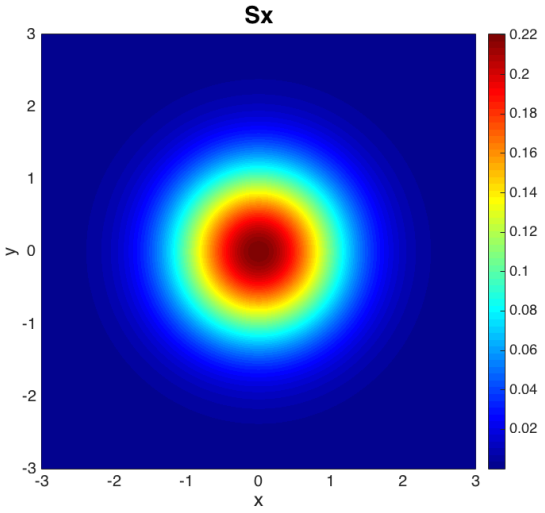

FIGURE 5.2: Spin component Sx in the ground state for the 2D spin-1 spinor ^{87}Rb BEC.

Fig. 5.2 looks practically as the ones in Fig. 5.1, but this is not a surprise, since the S_x component is a combination of the three components of the wavefunction solution of the equation, being the main difference the higher total intensity.

Being the interest of this thesis the study of the spin density vectors, Fig. 5.3 plots the spin vector in the xy-plane, which is the desired final output for each of the cases to be computed.

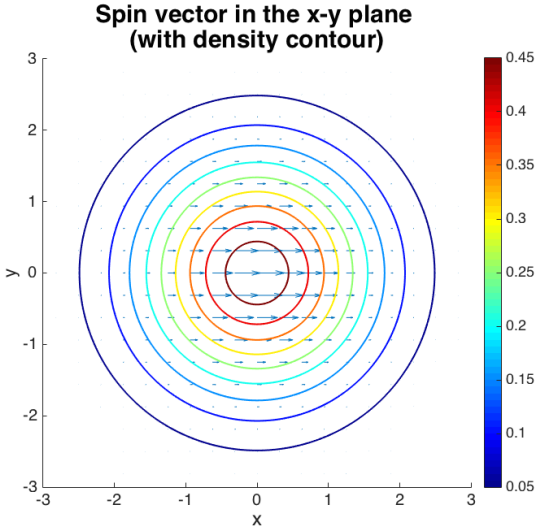

FIGURE 5.3: Spin density vector for the stationary state for the 2D spin-1 spinor ^{87}Rb BEC.

The density contour lines give an idea of the regions with higher or lower total wavefunction density (from the three components).

The insights of the dynamics of these kind of systems where there is no additional gradient or magnetic field can be of special interest, and it has been studied in the next section.

5.2.2 Model computation for the dynamics

The relaxation scheme is the numerical tool selected for the dynamics simulation, using GPELab. The description of this method was covered in the Sec. 4.1.2.1.

The total time of the evolution has been computed with a time step of $\Delta t = 0.001$ for the time discretisation, corresponding to 10 iterations. The CPU time for this calculation was about 12.89 minutes.

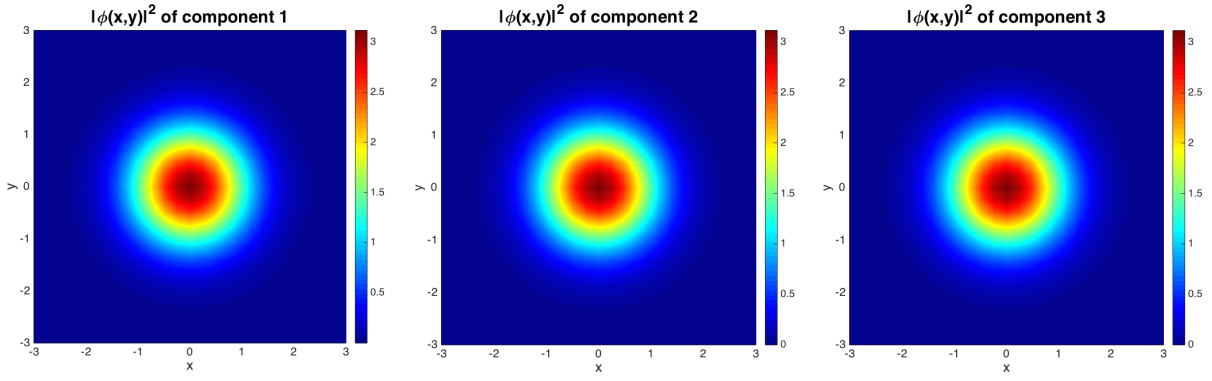

FIGURE 5.4: The 3 components of the ground state solution for the 2D spin-1 spinor ^{87}Rb BEC letting the system evolve with time.

Fig. 5.4 displays the modulus of the wavefunction for the solution of the ground state in the 3 components at the end of the evolution, and as expected, there is no particular change in any of the components, since there is no additional term that can affect the wavefunction of the ground state. However, extending the study to the spin density vector evolution, as in Fig. 5.5, it can be recognised that in fact, there is a small contraction of the high density vector contour.

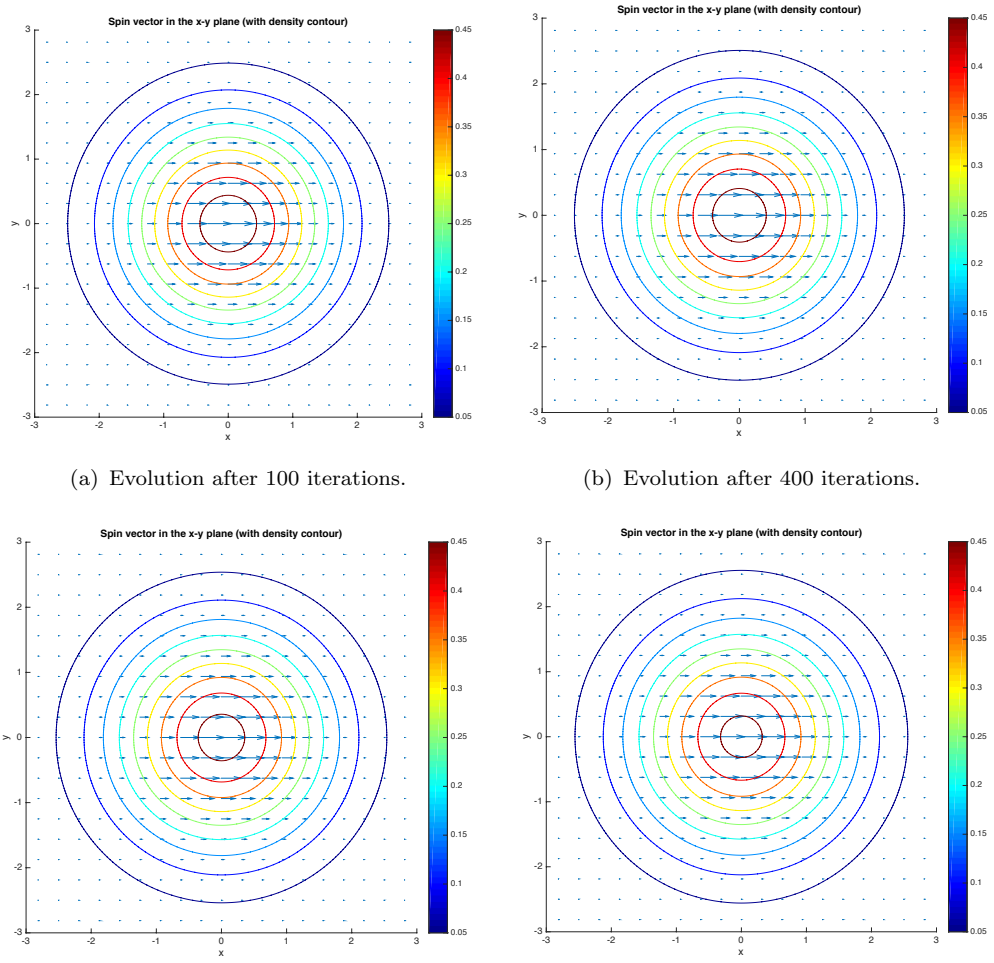

(a) Evolution after 100 iterations.

(b) Evolution after 400 iterations.

(c) Evolution after 700 iterations.

(d) Evolution after 1000 iterations.

FIGURE 5.5: Spin density vector evolution for the 2D spin-1 spinor ^{87}Rb BEC.

In the following section the results of the stationary solution as well as the dynamics by adding a magnetic field will be presented. Ultimately, the spin echo is going to be demonstrated.

5.3 Addition of a time-dependent magnetic field

In the last fifteen years few research papers have attempted the calculation of ground states for spin-1 spinors BECs in a presence of a magnetic field [40, 42–44].

The Hamiltonian for the $F = 1$ spinor BEC for a many-body system with a magnetic field will be represented by the Eq. 3.27, repeated below:

$$\hat{H} = \int \left[-\frac{\hbar^2}{2m}\nabla\psi_\alpha^*\nabla\psi_\alpha + V(\mathbf{r})\psi_\alpha^*\psi_\alpha - g\mu_B\psi_\alpha^*\mathbf{B}_i\mathbf{S}_{\alpha\beta}^i\Psi_\beta + \frac{1}{2}c_0\psi_\alpha^*\psi_{\alpha'}^*\psi_{\alpha'}\psi_\alpha + \frac{1}{2}c_2\psi_\alpha^*\psi_{\alpha'}\mathbf{S}_{\alpha\beta}\mathbf{S}_{\alpha'\beta'}\psi_{\beta'}\psi_\beta \right] d\mathbf{r} \tag{5.4}$$

The three coupled equations taking into account the magnetic field will result in:

$$i\frac{\partial}{\partial t}\psi_1(\mathbf{r},t) = \left[-\frac{1}{2}\nabla^2 + V(\mathbf{r}) + (\beta_n+\beta_s)(|\psi_1|^2+|\psi_0|^2) + (\beta_n-\beta_s)(|\psi_{-1}|^2 \right]\psi_1 + \beta_s\psi_{-1}^*\psi_0^2$$
$$- g\mu_B\mathbf{B}_1\left[cos(\gamma\mathbf{B}_0t)\mathbf{x} + isin(\gamma\mathbf{B}_0t)\mathbf{y}\right]\left[\frac{1}{\sqrt{2}}\psi_0\right] - g\mu_B\mathbf{B}_0\psi_1\mathbf{z}, \tag{5.5}$$

$$i\frac{\partial}{\partial t}\psi_0(\mathbf{r},t) = \left[-\frac{1}{2}\nabla^2 + V(\mathbf{r}) + (\beta_n+\beta_s)(|\psi_1|^2+|\psi_{-1}|^2) + \beta_n(|\psi_0|^2 \right]\psi_0 + 2\beta_s\psi_{-1}\psi_0^*\psi_1$$
$$- g\mu_B\mathbf{B}_1\left[cos(\gamma\mathbf{B}_0t)\mathbf{x} - isin(\gamma\mathbf{B}_0t)\mathbf{y}\right]\left[\frac{1}{\sqrt{2}}\psi_1\right] - g\mu_B\mathbf{B}_1\left[cos(\gamma\mathbf{B}_0t)\mathbf{x} + isin(\gamma\mathbf{B}_0t)\mathbf{y}\right]\left[\frac{1}{\sqrt{2}}\psi_{-1}\right], \tag{5.6}$$

$$i\frac{\partial}{\partial t}\psi_{-1}(\mathbf{r},t) = \left[-\frac{1}{2}\nabla^2 + V(\mathbf{r}) + (\beta_n+\beta_s)(|\psi_{-1}|^2+|\psi_0|^2) + ((\beta_n-\beta_s)(|\psi_1|^2 \right]\psi_{-1} + \beta_s\psi_0^2\psi_1^*$$
$$- g\mu_B\mathbf{B}_1\left[cos(\gamma\mathbf{B}_0t)\mathbf{x} - isin(\gamma\mathbf{B}_0t)\mathbf{y}\right]\left[\frac{1}{\sqrt{2}}\psi_0\right] + g\mu_B\mathbf{B}_0\psi_{-1}\mathbf{z}. \tag{5.7}$$

To be systematic in the calculations, the parameters must be defined for the atomic species of interest, that is, ^{87}Rb:

• The Bohr magneton will be set to 1 for the numerical simulation.

• The fine structure Landé g-factor for ^{87}Rb $5^2S_{1/2}$ is $\simeq 2$ [45], as the value for a BEC will be the one of the ground state of the atomic species.

The details and results of this computation are described next.

5.3.1 Model computation for the stationary solution

The system of coupled equations Eqs. 5.5-5.7 is the one employed for this computation without the time variant gradient, that is [46]:

$$i\frac{\partial}{\partial t}\psi_1(\mathbf{r},t) = \left[-\frac{1}{2}\nabla^2 + V(\mathbf{r}) + (\beta_n+\beta_s)(|\psi_1|^2+|\psi_0|^2) + (\beta_n-\beta_s)(|\psi_{-1}|^2\right]\psi_1 + \beta_s\psi_{-1}^*\psi_0^2 - g\mu_B\mathbf{B}_0\psi_1\mathbf{z}, \tag{5.8}$$

$$i\frac{\partial}{\partial t}\psi_0(\mathbf{r},t) = \left[-\frac{1}{2}\nabla^2 + V(\mathbf{r}) + (\beta_n+\beta_s)(|\psi_1|^2+|\psi_{-1}|^2) + \beta_n(|\psi_0|^2\right]\psi_0 + 2\beta_s\psi_{-1}\psi_0^*\psi_1, \tag{5.9}$$

$$i\frac{\partial}{\partial t}\psi_{-1}(\mathbf{r},t) = \left[-\frac{1}{2}\nabla^2 + V(\mathbf{r}) + (\beta_n+\beta_s)(|\psi_{-1}|^2+|\psi_0|^2) + ((\beta_n-\beta_s)(|\psi_1|^2\right]\psi_{-1} + \beta_s\psi_0^2\psi_1^* + g\mu_B\mathbf{B}_0\psi_{-1}\mathbf{z}. \tag{5.10}$$

The value of the parameters has been previously defined. The magnetic field is the only term not yet stated. The stationary states will have the following gradient magnetic field $\mathbf{B}_0$:

$$\mathbf{B}_0 = (1.5)\overline{\boldsymbol{z}}\ T. \tag{5.11}$$

A maximum of 10 iterations are evaluated with a discretised time step of $\Delta t = 0.1$. The CPU time for this calculation was about 12.36 seconds.

Fig. 5.6 represents the modulus of the wavefunction for the solution of the ground state in the 3 components, and the major discrepancy with the stationary state without magnetic field is the fact that the component 1, that is ψ_1, has a higher intensity that the other two, which appear to be very weak.

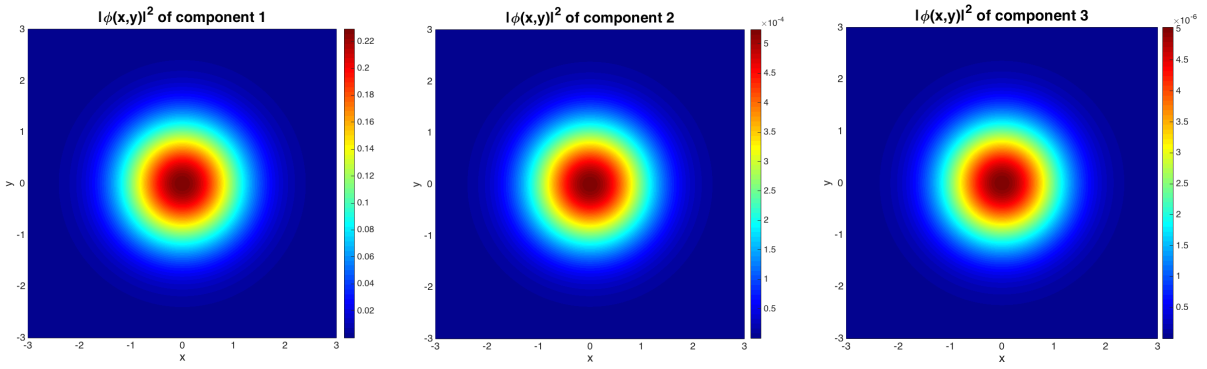

FIGURE 5.6: The 3 components of the ground state solution for the 2D spin-1 spinor ^{87}Rb BEC with additional magnetic field.

The spin Sx component has in this case a very low intensity, as Fig. 5.7 illustrates:

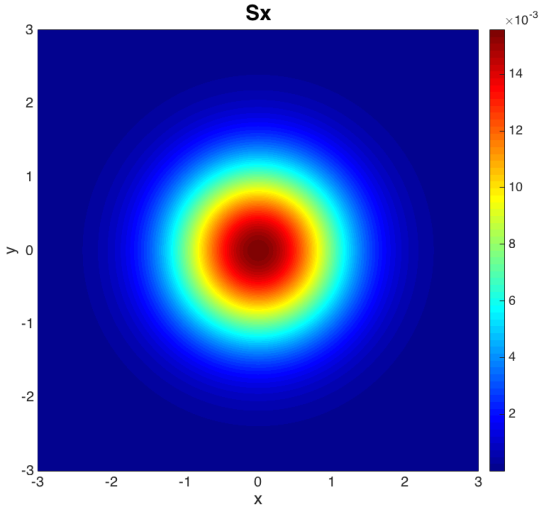

FIGURE 5.7: Spin component Sx in the ground state for the 2D spin-1 spinor ^{87}Rb BEC with additional magnetic field.

As the magnetic field acts in the z-axis, all spins have to be parallel to this axis, and a zero projection of the spins on the xy-plane is expected. However, Fig. 5.8 shows another result, due to the fact that all the simulations have been done in two dimensions, that is, the spin density vector on the z cannot be represented here in the xy-plane, which is by a similar result as the one without the magnetic field is obtained.

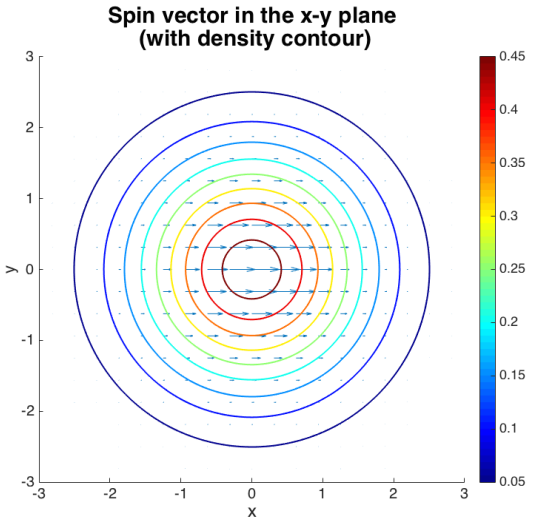

FIGURE 5.8: Spin vector in the xy-plane with additional magnetic field.

The next section is the most relevant within this research project, as contains the simulation results of the dynamic evolution of a spin-1 spinor BEC in the presence of a magnetic field applying a specific pulse sequence, the spin echo.

5.3.2 Spin echo dynamics

The dynamics of the system is described through the time dependent magnetic field represented by the following equation:

$$\mathbf{B} = \mathbf{B}_1 \left[cos(\gamma \mathbf{B}_0 t)\overline{\boldsymbol{x}} - sin(\gamma \mathbf{B}_0 t)\overline{\boldsymbol{y}} \right], \tag{5.12}$$

with $\mathbf{B}_1 = 0.1\mathbf{B}_0$ and γ is the gyromagnetic ratio, set to 1 for the numerics.

The results and details of the evolution are described below.

5.3.2.1 Model computation

For this simulation the system of coupled equations Eqs. 5.5-5.7 have been evaluated.

Repeatedly, a relaxation scheme is employed in the numerical tool for the dynamics simulation.

The time step chosen for the time discretisation has been $\Delta t = 0.001$ and the total time $\omega t = 20$. The CPU time for this calculation was about 4.15 hours.

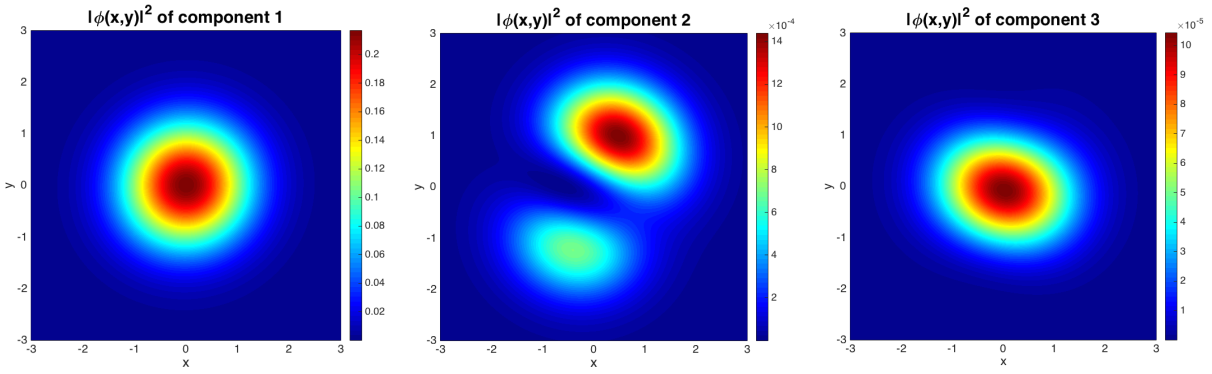

FIGURE 5.9: The 3 components of the ground state solution for the 2D spin-1 spinor ^{87}Rb BEC with additional magnetic field.

Fig. 5.9 illustrates the modulus of the three component of the wavefunction, where the first component has higher intensity value. Moreover, a distortion of the second a third component is observed.

The spin echo sequence is displayed in Fig. 5.10 with the dynamics of S projected on the xy-plane. The spins start to get oriented on the y-axis after the $\frac{\pi}{2}$ pulse (see figure Fig. 5.10 (a)), to continue precessing on the plane in (b) and (c). At a time $\omega t = 6.51$, the spins reverse the direction, after the π pulse is applied in (e). The coherence of the spins becomes observable through figures (f) and (g), and the spins will become refocussed almost at the end of the evolution, at $\omega t = 16.01$, as observed in figure (h).

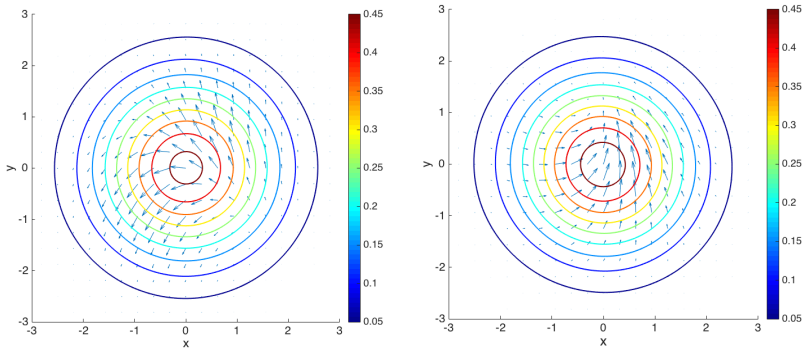

(a) $\omega t = 1.01$ (b) $\omega t = 2.51$

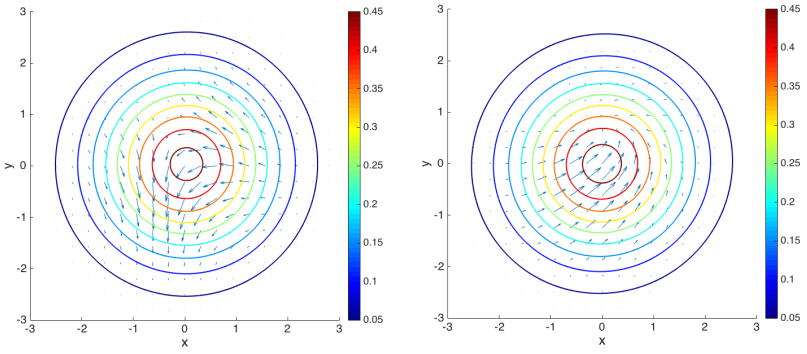

(c) $\omega t = 5.51$ (d) $\omega t = 6.51$

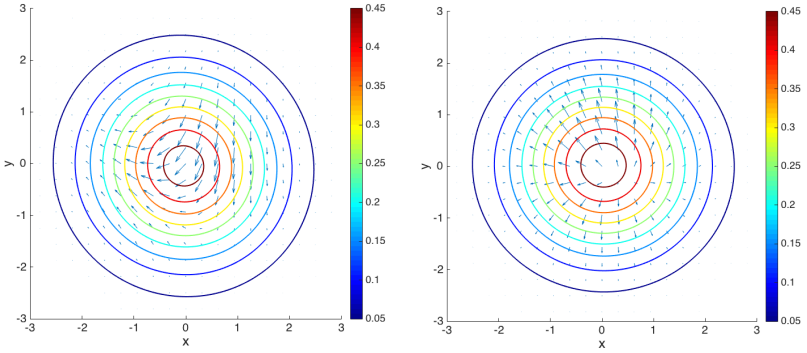

(e) $\omega t = 7.51$ (f) $\omega t = 9.01$

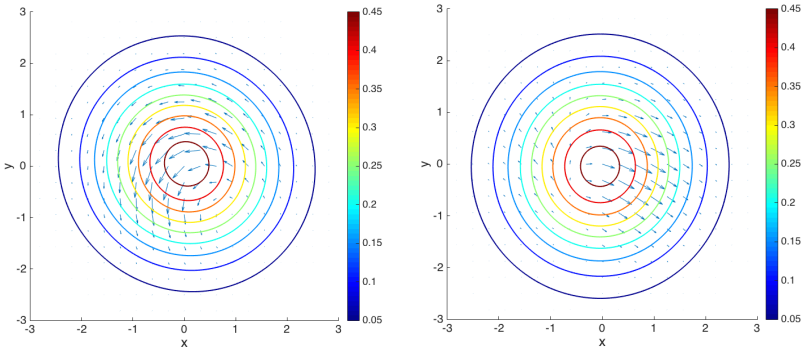

(g) $\omega t = 9.51$ (h) $\omega t = 16.01$

FIGURE 5.10: Spin echo time evolution of the spin density vectors S projected on the xy-plane.

5.4 Results discussion

In this chapter, the simulation results for the stationary solution as well as the dynamics of spin-1 spinor BEC have been proposed, to study the spin density vector evolution in the different cases proposed.

Using the numerical tool GPELab it is possible to simulate special cases of Schrödinger equations, mainly non linear ones, or Gross-Pitaevskii equations.

By having a ^{87}Rb BEC trapped by a harmonic potential, it is possible to represent the three different Zeemann states or couple wavefunction equations.

The three components of the resulting wavefunction in the different models have been analysed, showing very interesting discrepancies when the system evolves in time.

As well, the spin density vector has been represented, as the main focus for this research.

At first, without any additional term, the stationary solution as well as the dynamics of the system has been evaluated, curiously highlighting a small contraction of the high density vector contour in the spin density vector representation at the end of the evolution.

Secondly, by adding a magnetic field, the system has been evaluated in two cases: a stationary state with a magnetic field in the z direction, and the dynamics under a spin echo sequence represented by a time variant gradient in x and y axis. The application of a magnetic field in the stationary state is mainly observed under the difference in intensity within the three components of the wavefunction.

The most interested behaviour appears when a time variant magnetic field is applied. A distortion occurs with time in the second and third components of the wavefunction.

Also in the last section, the specific study of the spin echo applied to this type of BEC have been demonstrated, where the spin time development is clearly observed in Fig. 5.10.

It is important to meantion here the discrepancies that can be found between these results and the previous results from Yasunaga and Tsubota papers [5, 6], considering:

- only short range interactions have been taking into account during all the simulations,

- there are always small errors associated to any numerical computation. Therefore, numerical errors is probably the main reason on the differences obtained,

- as well, there is no detail of the numerical method employed by the authors, which leads to obvious variation in the results,

- last but not least, the value of the different parameters can vary, resulting in small discrepancies during the dynamics evolution.

In summary, the application of special radio-frequency techniques, as spin echo, can be observed in a variety of physical models, and by using different numerical tools.

It is indeed very interesting to see how these kind of magnetic field affects the spin density. Nonetheless, the possibility to observe how a pulse sequence effects the wavefunction offers a new picture of the insights of matter a very cold temperatures, and can be applied to numerous experiments and fields in the very near future.

Part V

Conclusions

Chapter 6

Outlook and conclusions

6.1 Outlook

As a future direction of this research, the cases where also long range interactions are present can be investigated, by including the dipolar constant term in the coupled equations. There is a number of research papers with the focus on spinor dipolar Bose-Einstein condensates [5, 47–49].

Magnetic characterisation is another field in physics that benefits from magnetic resonance in very cold temperature systems, as it has been already described in [49].

An important application of spin-echo is found in magnetometry, where very weak magnetic fields are detected [50]. Perhaps spin echo magnetometry based in very low temperatures will be a new resource in the field of medicine.

An alternative approach for these simulations could be by employing wavelets. There are early discussions in the scientific community about the possible advantage of using these mathematical functions in the field of cold atoms.

6.2 Conclusions

The realization of spin echo in a spinor Bose–Einstein condensate (BEC) has been previously proposed theoretically and numerically by Yasunaga and Tsubota [5, 6]. However, the method used was not clear and the details of the algorithm have not been discussed.

In this document the application of an important and precise pulse sequence, spin echo, to a specific type of Bose-Einstein condensate, a spin-1 spinor, has been studied. The simulations have been computed applying numerical algorithms, by making use for the first time in these kind of problems of GPELab, a $MATLAB^{®}$ toolbox developed to model non linear Schrödinger equations, the so called Gross-Pitaevskii equations.

Simulating the dynamics of spinor BECs, it has been possible to study the behaviour of the wavefunction components as well as the dynamics of the spin density vector with and without an additional magnetic field.

The simulations presented in this thesis are directly relevant to some ongoing experiments, as deduced from several papers mentioned in the text, and fundamentally interesting in terms of the dynamics of specific systems under a sequence of radio-frequency pulses. It would be necessary to make a further study for other systems, perhaps by changing the magnetic fields, or by using other numerical algorithms. Furthermore, other atomic species, or molecules, must be simulated in order to broaden the fields of interest. Moreover, the simulation of a BEC in three dimensions could reveal very interesting perspectives in terms of spin dynamics under certain radio-frequency pulses. Other alternatives such as Carr and Purcel [14] sequence proposals could be indeed applied to low temperature physics.

The research insights presented here are very useful for further theoretical and experimental work. Although just a small contribution in this area fell within the scope of this work, it has been clearly demonstrated that medical imaging techniques can be applied to other kind of systems, as the ones simulated in this thesis, directly impacting other areas of physics.

Bibliography

[1] S.G. Odaibo. *Quantum Mechanics and the MRI Machine.* Symmetry Seed Books, 2012.

[2] M. A. Brown and R. C. Semelka. *MRI Basic Principles and Applications.* John Wiley and Sons, 2003.

[3] D. Weishaupt, J.M. Froehlich, D. Nanz, V.D. Köchli, K.P. Pruessmann, and B. Marincek. *How does MRI work?: An Introduction to the Physics and Function of Magnetic Resonance Imaging.* Lecture notes in mathematics. Springer Berlin Heidelberg, 2008.

[4] K. Toyoda, Y. Takahashi, and T. Yabukazi. Magnetic resonance imaging of bose–einstein condensates. *Appl. Phys. B*, **74**:115–120, 2002.

[5] M. Yasunaga and M. Tsubota. Spin echo in spinor dipolar bose-einstein condensates. *Phys. Rev. Lett.*, **101**:220401, Nov 2008.

[6] M. Yasunaga and M. Tsubota. Magnetic resonance, especially spin echo, in spinor bose-einstein condensates. *Journal of Physics: Conference Series*, **150**(3):032127, 2009.

[7] X. Antoine and R. Duboscq. Gpelab, a matlab toolbox to solve gross-pitaevskii equations ii: Dynamics and stochastic simulations. *Computer Physics Communications*, **193**:95 – 117, 2015.

[8] K. Krane. *Modern Physics.* John Wiley and Sons, 1996.

[9] C. J. Pethick and H. Smith. *Bose-Einstein condensation in dilute gases.* Cambridge University Press, second edition, 2008.

[10] C. Westbrook. *MRI at a Glance.* Wiley, 2002.

[11] A. Santos. *Basic MRI Physics*. Lecture Notes, Erasmus Course on Magnetic Resonance Imaging, Universidad Politécnica de Madrid, Oct 2014.

[12] W. A. Gibby. Basic principles of magnetic resonance imaging. **16**:1–64, 2005.

[13] E. L. Hahn. Spin echoes. *Phys. Rev.*, **80**:580–594, Nov 1950.

[14] H. Y. Carr and E. M. Purcell. Effects of diffusion on free precession in nuclear magnetic resonance experiments. *Phys. Rev.*, **94**:630–638, May 1954.

[15] J. Wolters. *Integrated Quantum Hybrid Systems*. Pan Stanford Publishing, 2015.

[16] T. Lahaye, C. Menotti, L. Santos, M. Lewenstein, and T. Pfau. The physics of dipolar bosonic quantum gases. *Reports on Progress in Physics*, **72**(12):126401, 2009.

[17] A. J. Daley. *The Physics of Cold Atoms*. Lecture Notes, University of Innsbruck, 2008.

[18] F. Dalfovo, S. Giorgini, L. P. Pitaevskii, and S. Stringari. Theory of bose-einstein condensation in trapped gases. *Rev. Mod. Phys.*, **71**:463–512, Apr 1999.

[19] Y. Castin. Bose-einstein condensates in atomic gases: simple theoretical results. *arXiv*, **cond-mat/0105058**, May 2001.

[20] T-L. Ho. Spinor bose condensates in optical traps. *Phys. Rev. Lett.*, **81**:742–745, Jul 1998.

[21] J. Stenger, S. Inouye, D. M. Stamper-Kurn, H.-J. Miesner, A. P. Chikkatur, and W. Ketterle. Spin domains in ground-state Bose-Einstein condensates. *Nature*, **396** (6709):345–348, Nov 1998.

[22] D. Cao, I-L. Chern, and J-C. Wei. On ground state of spinor bose–einstein condensates. *Nonlinear Differential Equations and Applications NoDEA*, **18**(4):427–445, 2011.

[23] D. M. Stamper-Kurn and M. Ueda. Spinor bose gases: Symmetries, magnetism, and quantum dynamics. *Rev. Mod. Phys.*, **85**:1191–1244, Jul 2013.

[24] D. Yan and T. Ma. The gross-pitaevskii model of spinor bec. *Journal of Applied Mathematics*, **2012**, 2012.

[25] C. K. Law, H. Pu, and N. P. Bigelow. Quantum spins mixing in spinor bose-einstein condensates. *Phys. Rev. Lett.*, **81**:5257–5261, Dec 1998.

[26] T. Ohmi and K. Machida. Bose-einstein condensation with internal degrees of freedom in alkali atom gases. *Journal of the Physical Society of Japan*, **67**(6):1822–1825, 1998.

[27] D. E. Chang. Method for monopole creation in spinor bose-einstein condensates. *Phys. Rev. A*, **66**:025601, Aug 2002.

[28] Y. Kawaguchi and M. Ueda. Spinor bose-einstein condensates. *arXiv*, **1001.2072v3**, May 2012.

[29] X. Antoine and R. Duboscq. *Modeling and Computation of Bose-Einstein Condensates: Stationary States, Nucleation, Dynamics, Stochasticity*, pages 49–145. Springer International Publishing, 2015.

[30] W. Bao and Q. Du. Computing the ground state solution of bose–einstein condensates by a normalized gradient flow. *SIAM Journal on Scientific Computing*, **25**(5): 1674–1697, 2004.

[31] X. Antoine and R. Duboscq. Gpelab, a matlab toolbox to solve gross-pitaevskii equations i: Computation of stationary solutions. *Computer Physics Communications*, **185**(11):2969 – 2991, 2014.

[32] Drake, editor. *Springer handbook of atomic, molecular, and optical physics*, pages 1219–1234. Springer, 2006.

[33] C.F. Gerald, P.O. Wheatley, H.V. Velázquez, and J.C.V. Sotelo. *Análisis numérico con aplicaciones*. Pearson educación. 2000.

[34] C. Besse. A relaxation scheme for the nonlinear schrödinger equation. *SIAM Journal on Numerical Analysis*, **42**(3):934–952, 2005.

[35] X. Antoine, W. Bao, and C. Besse. Computational methods for the dynamics of the nonlinear schrödinger/gross-pitaevskii equations. *Computer Physics Communications*, **184**(12):2621 – 2633, 2013.

[36] W. Zhang and L. You. An effective quasi-one-dimensional description of a spin-1 atomic condensate. *Phys. Rev. A*, **71**:025603, Feb 2005.

[37] W. Bao and H. Wang. A mass and magnetization conservative and energy-diminishing numerical method for computing ground state of spin-1 bose-einstein condensates. *SIAM Journal on Numerical Analysis*, **45**(5):2177–2200, 2007.

[38] X. Han and B. Wu. Ehrenfest breakdown of the mean-field dynamics of bose gases. *Phys. Rev. A*, **93**:023621, Feb 2016.

[39] W. Bao, I-l. Chern, and F. Y. Lim. Efficient and spectrally accurate numerical methods for computing ground and first excited states in Bose-Einstein condensates. *Journal of Computational Physics*, **219**(2):836–854, 2006.

[40] W. Bao, I-l. Chern, and Y. Zhang. Efficient numerical methods for computing ground states of spin-1 bose-einstein condensates based on their characterizations. *Journal of Computational Physics*, **253**:189 – 208, 2013.

[41] J-H. Chen, I-L. Chern, and W. Wang. Exploring ground states and excited states of spin-1 bose-einstein condensates by continuation methods. *Journal of Computational Physics*, **230**(6):2222 – 2236, 2011.

[42] W. Zhang, S. Yi, and L. You. Mean field ground state of a spin-1 condensate in a magnetic field. *New Journal of Physics*, **5**(1):77, 2003.

[43] F. Y. Lim and W. Bao. Numerical methods for computing the ground state of spin-1 bose-einstein condensates in a uniform magnetic field. *Phys. Rev. E*, **78**:066704, Dec 2008.

[44] Michał Matuszewski. Ground states of trapped spin-1 condensates in magnetic field. *Phys. Rev. A*, **82**:053630, Nov 2010.

[45] D. A. Steck. Rubidium 87 d line data. URL:http://steck.us/alkalidata/rubidium87numbers.pdf, 2015.

[46] R. S. Tasgal and Y. B. Band. Continuous-wave solutions in spinor bose-einstein condensates. *Phys. Rev. A*, **87**:023626, Feb 2013.

[47] M. Takahashi, S. Ghosh, T. Mizushima, and K. Machida. Spinor dipolar bose-einstein condensates: Classical spin approach. *Phys. Rev. Lett.*, **98**:260403, Jun 2007.

[48] Y. Kawaguchi, H. Saito, and M. Ueda. Can spinor dipolar effects be observed in bose-einstein condensates? *Phys. Rev. Lett.*, **98**:110406, Mar 2007.

[49] M. Yasunaga and M. Tsubota. Ferromagnetic resonance in spinor dipolar bose-einstein condensates. *Phys. Rev. A*, **83**:013618, Jan 2011.

[50] Y. Eto, H. Ikeda, H. Suzuki, S. Hasegawa, Y. Tomiyama, S. Sekine, M. Sadgrove, and T. Hirano. Spin-echo-based magnetometry with spinor bose-einstein condensates. *Phys. Rev. A*, **88**:031602, Sep 2013.